Thermal Energy Storage (TES) Modeling and Design

Cooperative Research and Development Final Report

CRADA Number: CRD-19-00789

NREL Technical Contact: Jason Woods

NREL is a national laboratory of the U.S. Department of Energy
Office of Energy Efficiency & Renewable Energy
Operated under Contract No. DE-AC36-08GO28308

This report is available at no cost from the National Renewable Energy Laboratory (NREL) at www.nrel.gov/publications.

Technical Report
NREL/TP-5500-93359
June 2025

Thermal Energy Storage (TES) Modeling and Design

Cooperative Research and Development Final Report

CRADA Number: CRD-19-00789

NREL Technical Contact: Jason Woods

Suggested Citation
Woods, Jason. 2025. *Thermal Energy Storage (TES) Modeling and Design: Cooperative Research and Development Final Report, CRADA Number CRD-19-00789.* Golden, CO: National Renewable Energy Laboratory. NREL/TP-5500-93359. https://www.nrel.gov/docs/fy25osti/93359.pdf.

NREL is a national laboratory of the U.S. Department of Energy
Office of Energy Efficiency & Renewable Energy
Operated under Contract No. DE-AC36-08GO28308

This report is available at no cost from the National Renewable Energy Laboratory (NREL) at www.nrel.gov/publications.

Technical Report
NREL/TP-5500-93359
June 2025

National Renewable Energy Laboratory
15013 Denver West Parkway
Golden, CO 80401
303-275-3000 • www.nrel.gov

NOTICE

This work was authored by the National Renewable Energy Laboratory for the U.S. Department of Energy (DOE) under Contract No. DE-AC36-08GO28308. Funding provided by U.S. Department of Energy Office of Energy Efficiency and Renewable Energy Building Technologies Office. The views expressed herein do not necessarily represent the views of the DOE or the U.S. Government.

This work was prepared as an account of work sponsored by an agency of the United States Government. Neither the United States Government nor any agency thereof, nor any of their employees, nor any of their contractors, subcontractors or their employees, makes any warranty, express or implied, or assumes any legal liability or responsibility for the accuracy, completeness, or any third party's use or the results of such use of any information, apparatus, product, or process disclosed, or represents that its use would not infringe privately owned rights. Reference herein to any specific commercial product, process, or service by trade name, trademark, manufacturer, or otherwise, does not necessarily constitute or imply its endorsement, recommendation, or favoring by the United States Government or any agency thereof or its contractors or subcontractors. The views and opinions of authors expressed herein do not necessarily state or reflect those of the United States Government or any agency thereof, its contractors or subcontractors.

This report is available at no cost from the National Renewable Energy Laboratory (NREL) at www.nrel.gov/publications.

U.S. Department of Energy (DOE) reports produced after 1991 and a growing number of pre-1991 documents are available free via www.OSTI.gov.

Cover photos (clockwise from left): Josh Bauer, NREL 61725; Visualization from the NREL Insight Center; Getty-181828180; Agata Bogucka, NREL 91683; Dennis Schroeder, NREL 51331; Werner Slocum, NREL 67842.

NREL prints on paper that contains recycled content.

Cooperative Research and Development Final Report

Report Date: February 7, 2025

In accordance with requirements set forth in the terms of the CRADA agreement, this document is the CRADA final report, including a list of subject inventions, to be forwarded to the DOE Office of Scientific and Technical Information as part of the commitment to the public to demonstrate results of federally funded research.

Parties to the Agreement: NETenergy LLC

CRADA Number: CRD-19-00789

CRADA Title: Thermal Energy Storage (TES) Modeling and Design

Responsible Technical Contact at Alliance/National Renewable Energy Laboratory (NREL):

Jason Woods | jason.woods@nrel.gov

Name and Email Address of POC at Company:

Said Al-Hallaj | said@netenergytes.com

Sponsoring DOE Program Office(s):

Office of Energy Efficiency and Renewable Energy (EERE), Building Technologies Office

Joint Work Statement Funding Table showing DOE commitment:

The partner's funds are not published in this report. State "No NREL Shared Resources" here if true.

Estimated Costs	NREL Shared Resources a/k/a Government In-Kind
Year 1	$250,000.00
Year 2, Modification #1	$250,000.00
Year 3, Modification #2	$0.00
Year 4, Modification #3	$0.00
TOTALS	$500,000.00

This report is available at no cost from the National Renewable Energy Laboratory (NREL) at www.nrel.gov/publications.

Executive Summary of CRADA Work:

This project will assess the performance of an innovative high efficiency air conditioner integrated with a composite phase change material (PCM). The research will address critical electric grid challenges by evaluating the thermal efficiency and load-shifting capabilities in NREL's HVAC characterization lab.

Task #	Task Title	Expected Results
1	Modeling and design	HVAC system design, including PCM thermal storage module
2	Prototype characterization experiments	Lab characterization of gen-1 prototype (composite PCM thermal storage module and HVAC system)
3	Gen-2 design	Updated models; 2nd generation design of composite PCM thermal storage module; modifications, as needed, to HVAC system prototype
4	Gen-2 prototype characterization and integration experiments	Characterization of 2nd generation prototype (new bench-scale composite PCM thermal storage module)
5	Building modeling and scenario simulations	Building simulation tool; Scenario simulation results
6	Path to Market	Technical feature requirements for market penetration and establishing pathways through utilities and key trade organizations to spread the awareness of the technology.
7	Final Evaluation	Evaluate lab characterization and integration results Final reporting and next steps Go/No-go decision for pilot testing
8	Modeling and design of high-power PCM heat exchanger	Modeling results through .pptx slides Design specifications for two prototypes: (1) a 1 kWh, 25 kW system used with R410a, (2) a ~0.1 kWh, 1 kW system with glycol
9	Bench-scale experimental validation	Experimental results of prototype (2) from task 8 using glycol

CRADA benefit to DOE, Participant, and US Taxpayer:

- Assists laboratory in achieving programmatic scope, and/or
- Uses the laboratory's core competencies, and/or
- Enhances U.S. competitiveness by utilizing DOE developed intellectual property and/or capabilities.

This report is available at no cost from the National Renewable Energy Laboratory (NREL) at www.nrel.gov/publications.

Summary of Research Results:

Task 1: Modeling and design

Task Summary: *Under this task, NREL will develop and improve upon models at the component and system level. These models will be used to help design a composite PCM thermal storage module and an HVAC system prototype integrated with the thermal storage module. The full system design and specifications will be delivered by NREL based on the modeling results, along with input from NET Energy and their Original Equipment Manufacturer (OEM) partners*.

NETenergy designed and fabricated five prototype TES modules for experimental evaluation. Figure 1 shows a 3-D CAD drawing and photograph of one module. The module consists of 12 slabs of composite PCM with alternating discharge (22% Ethylene Glycol) and charge (R410a) fluid circuits. The dimensions of an individual slab are 0.520 m × 0.460 m × 0.035 m (L×W×H). Copper tubes of 0.0095 m (3/8 in) outer diameter were used for both fluid circuits. The fluid circuits formed a 20-pass serpentine path in each row. A total of 13 tubes (7 discharge, 6 charge) were used. There were 7 single-pass discharge circuits and 2 three-pass charge circuits. The design of the thermal energy storage (TES) modules rely on the thermal conduction path between the two fluid circuits. Thus, the thermal conduction of the graphite foam along with the contact conductance between the copper tubes and the composite material are critical factors in the performance of this design. For the system to operate efficiently, these conductance values should be maximized.

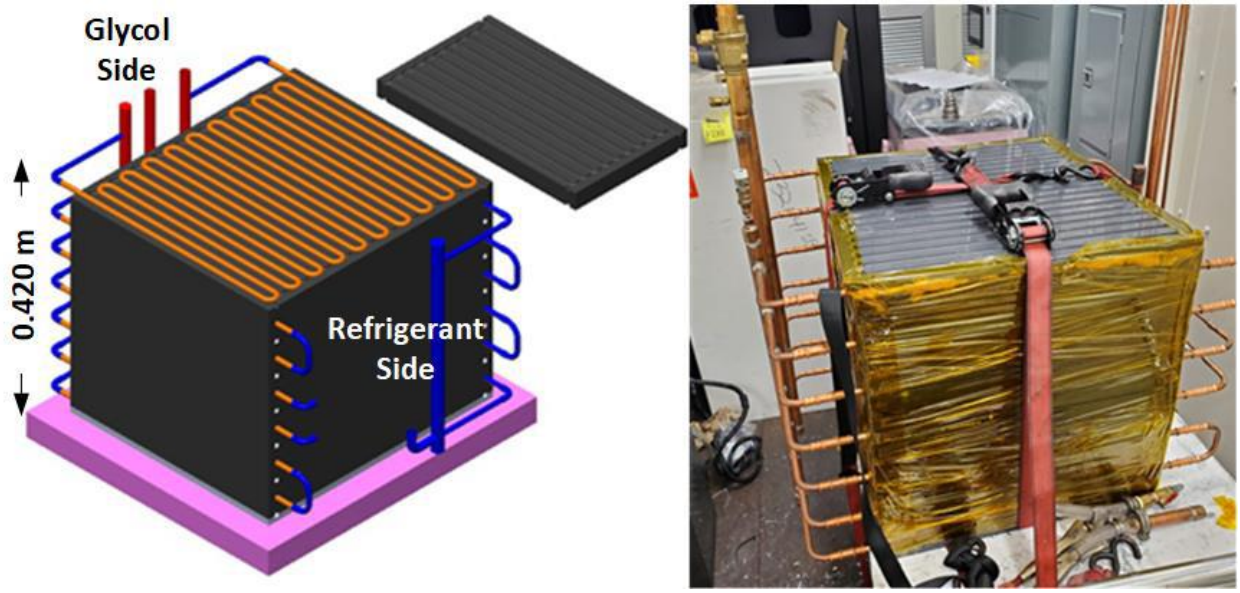

Figure 1: 3-D CAD rendering (left) and the fabricated thermal energy storage module (right)

This report is available at no cost from the National Renewable Energy Laboratory (NREL) at www.nrel.gov/publications.

We assumed the following to simplify the governing equations:

- fluid flow is assumed to be one-dimensional and incompressible
- viscous dissipation and body forces are neglected,
- dynamic variations in pressure are neglected and a static formulation of pressure loss is used over each control volume during every time step,
- effects of axial conduction are neglected in the fluid as the Peclet (Pe) number is typically large,
- constant cross-sectional area of fluid flow,
- uniform heat transfer coefficient assumed in the control volume for both fluids,
- refrigerant flow is assumed to be at quasi-steady state with saturated vapor at the outlet of the module,
- heat transfer in the composite PCM is modeled as two-dimensional conduction from the adjacent nodes,
- The graphite-tetradecane composite is modeled as a single material with one set of material properties,
- lumped capacitance is used for each PCM volume,
- heat transfer from curved tube surface to the PCM is modeled using an empirical shape factor for heat conduction, and
- finite thermal contact resistance is used at the interface between the tube and the PCM volume and between PCM volumes.

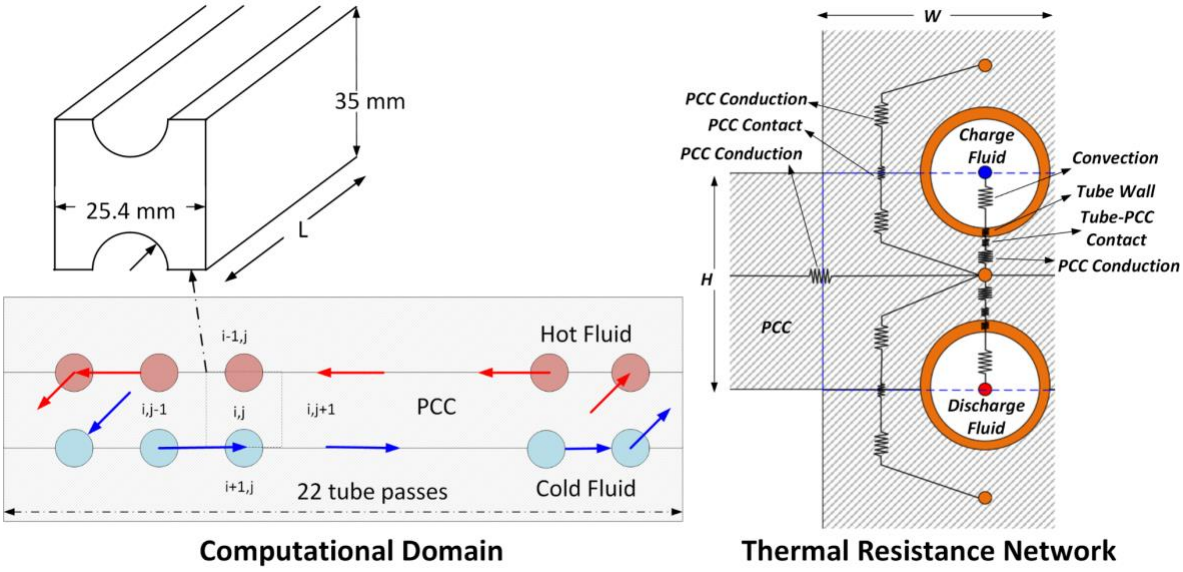

Figure 2: Computational domain and thermal resistance network

These assumptions simplify the conservation laws and the energy conservation equations for the two fluids and the composite PCM, and the static pressure drop equation is used per node to formulate the system of discretized equations. We use a thermal resistance network formulation to resolve different convective and conductive heat transfer media. Figure 2 shows a single control volume with both fluid tubes and the PCM volume.

This report is available at no cost from the National Renewable Energy Laboratory (NREL) at www.nrel.gov/publications.

This thermal storage was combined with two other subsystems: a charging unit, a discharging unit, and the NETenergy thermal energy storage (Figure 3).

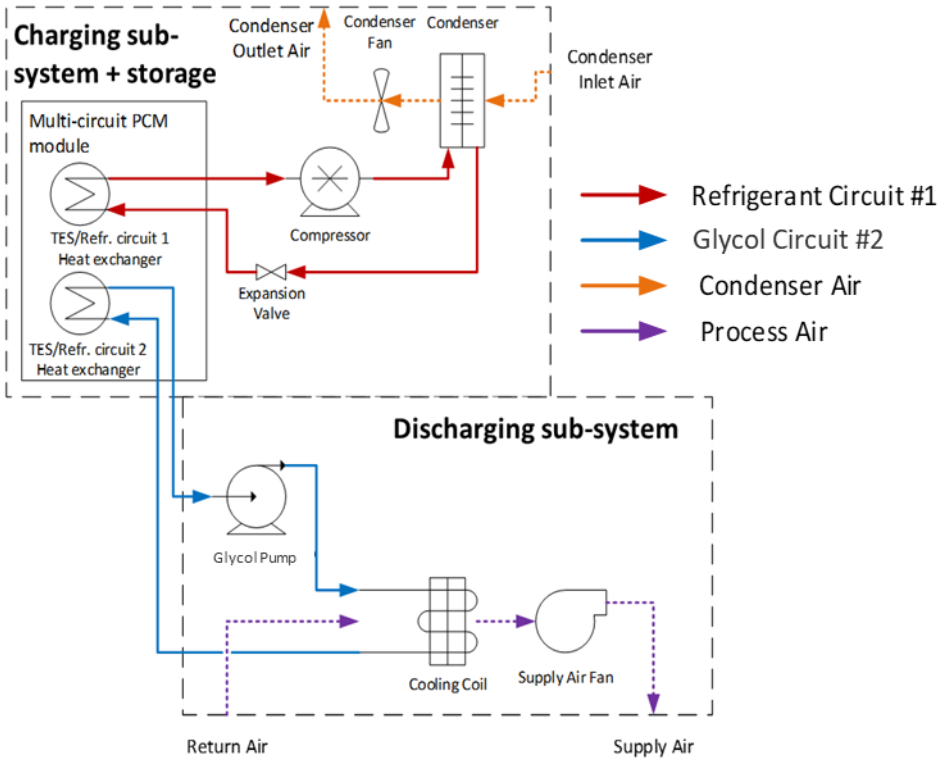

Figure 3: System schematic of air-conditioner with thermal energy storage

The **charge sub-system** delivers high pressure liquid to the TES and receives low pressure vapor back from the TES. The subsystem consists of a re-purposed split system condensing unit, a nominal 17.6 kW_t condensing unit manufactured by Trane. The condensing unit was modified with a ZPV038 series variable speed compressor, liquid-line heat exchanger and a refrigerant accumulator internal to the condensing unit. The system also had a suite of sensors pre-installed to measure refrigerant temperatures, pressures, and mass flow rate. The design intent of this subsystem was to be a flexible platform to perform experiments. The charging subsystem allows for variable control of the charging to one of several modes:

1. Constant charging capacity – maintain a constant heat removal rate
2. Constant charging temperature – maintain a constant evaporator saturated temperature
3. Constant volumetric capacity – mimic a single- or multi-speed compressor

The liquid line heat exchanger and integrated accumulator were placed to add refrigerant gas superheating and avoid transient liquid bursts from entering the compressor. Initial modeling suggested that evaporator saturated temperature can be maintained several degrees Celsius higher by using a liquid line heat exchanger. This is because both the thermal energy storage and refrigerant boiling are a near-isothermal process and can be as close as 2 °C temperature difference. Thus, there is not enough temperature difference to provide a safe level of superheat into the compressor.

This report is available at no cost from the National Renewable Energy Laboratory (NREL) at www.nrel.gov/publications.

The **discharge sub-system** cools a building space using a standard chilled glycol coil. Since refrigeration temperatures were expected to be as low as -8°C during experiments, 22% ethylene glycol was used. This subsystem consists of a coil, variable speed glycol pump, and pair of variable speed fans packaged in an air handling unit. The design intent was to receive 8°C chilled glycol from the TES to cool 3398 SCMH (2000 CFM) of process air to provide 17.6 kW_{th} of cooling. Because the TES delivers relatively constant temperature glycol, capacity modulation is accomplished by modulating air and glycol flow rates. Reducing air and glycol flow during lower-load conditions thus translate to air temperature and humidity dropping below that of the design condition. This provides the benefit of delivering air at a dewpoint less than about 13°C at all operating points and maintaining an acceptably low sensible heat ratio (ratio of sensible heat removal to total heat removal). This combination of modulation capacity (down to about 20% of full load capacity) and constant supply air dewpoint creates a system with good humidity control. In hot/dry climates, where humidity control is not a primary concern, air flow rate can be increased to maintain total capacity and deliver a higher sensible heat ratio.

The **dual-circuit thermal energy storage modules** functions as a thermal buffer between the charge and discharge sub-systems. The modules allow the system to follow building thermal loads and maintain thermal comfort of the occupants while managing energy and power draw from the electric grid. The modules contained 24.2 kWh (6.9 tonh) of thermal storage capacity calculated from an isothermal temperature from -2°C to 15°C. The modules have two distinct fluid circuits that function to thermally connect the phase change material, the glycol stream, and the refrigerant stream (evaporator). Ideally, when in operation, all exiting fluid temperatures match each other and the temperature of the PCM. However, this would require an un-attainable 100% effective heat exchange process. In the prototype design, the TES heat exchanger was dictated by existing manufacturing constraints and consisted of the serpentine design discussed above. The repeating stacking of the tubes and composite PCM was as follows: glycol serpentine – 35mm PCM slab – refrigerant serpentine – 35 mm PCM slab. The thermal network dictates that the heat flow from the glycol, through the composite PCM, and into the refrigerant.

The prototype system design allowed for measured thermal performance of each of the sub-systems, and to discover the aspects that work well and those that require improvement. Given this, the system design was intended to provide the following functionality:

1. 17.6 kWth net cooling capacity at AHRAE standard conditions
2. > 1.2 hours of thermal energy storage
3. During full load hybrid mode, the TES should provide at least 1/3 of the peak cooling capacity throughout its discharge. This equates to delivering 10 °C chilled water at a discharge rate of ~ 6 kWth down to 10% SOC.
4. Efficient TES module charging is critical to overall energy use and utility costs. The TES was designed to maintain less than 5°C approach between refrigerant evaporator temperature and the TES module temperature at 17.6 kWt charge capacity.

This report is available at no cost from the National Renewable Energy Laboratory (NREL) at www.nrel.gov/publications.

The refrigeration cycle efficiency is sensitive to the saturated evaporator temperature; every 1 °C drop in evaporator temperature increases energy use by 0.03 kW/ton. A system with a seasonal energy efficiency rating (SEER) of 18 btu/Wh consumes 0.667 kW/ton seasonally (kW/ton = 12 / SEER). Thus a drop by 1°C in seasonally averaged evaporator temperature results in about 4.5% increase in seasonal energy. This penalty is inherent in an air conditioning system with a secondary fluid. Minimizing its effect is critical toward managing energy and power use. However, the thermal storage allows charging during cooler periods of the day, which can help mitigate this penalty. This is illustrated in the following system-level data and system modeling in the remainder of this report.

Task 2: Prototype characterization experiments

Task Summary: *Under this task, NET Energy and its OEM partners will fabricate prototypes of the PCM thermal storage modules and HVAC systems based on task-1 specifications and deliver them to NREL. NREL will characterize the performance of these prototypes in its laboratory, share these results with NET Energy and HVAC OEM, and use the results to validate or update their numerical models.*

NETenergy fabricated five thermal energy storage modules to be coupled with the charging and discharging sub-systems. The complete system was installed at the HVAC Laboratory at NREL for performance characterization. Figure 3 shows a schematic of the setup in the lab. Thermal energy storage modules (Figure 4) were connected to the refrigeration system (charging circuit) and the air-handling system coupled through a water-glycol loop (discharge circuit). We instrumented the refrigeration system, air-handling system, glycol circuit, and the thermal energy storage modules to measure various temperatures, pressures, flow rates in the system (Figure 5) to calculate heat transfer rates and characterize system performance. All measurement probes and actuators were connected to the data acquisition and control system in the laboratory to collect experimental data and implement control algorithms.

The laboratory can provide air at the desired temperature and humidity to simulate different indoor and outdoor conditions. Airstreams were connected to the charge- and discharge-side of the system with measurements of dry bulb and dew point temperature, and volumetric flow rates. Pressure and temperature probes at several locations of the refrigerant circuit allowed us to fully define the thermodynamic state of the working fluid. With the measured mass flow rate of the refrigerant, the heat transfer rate in an individual component is estimated as:

$$\dot{Q}_{ref} = \dot{m}_{ref}(|h_{ref,out} - h_{ref,in}|)$$

This report is available at no cost from the National Renewable Energy Laboratory (NREL) at www.nrel.gov/publications.

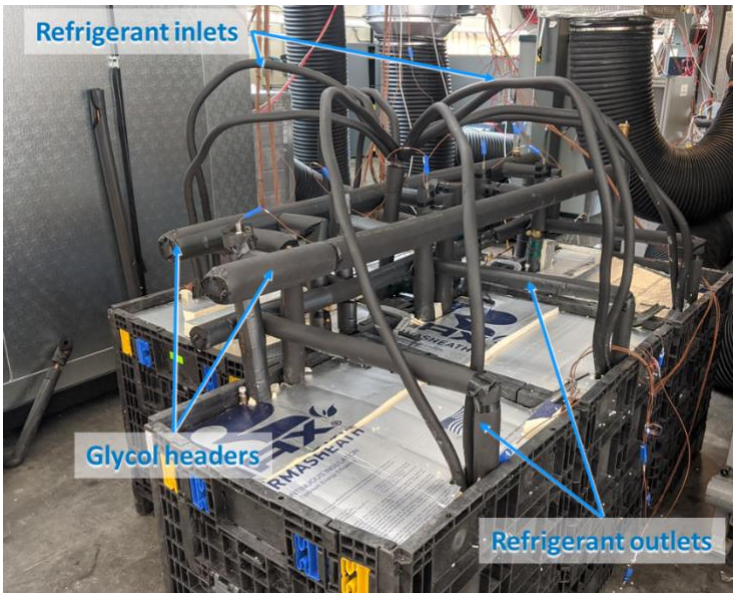

Figure 4: Thermal energy storage modules connected to the air-conditioning and air-handling system

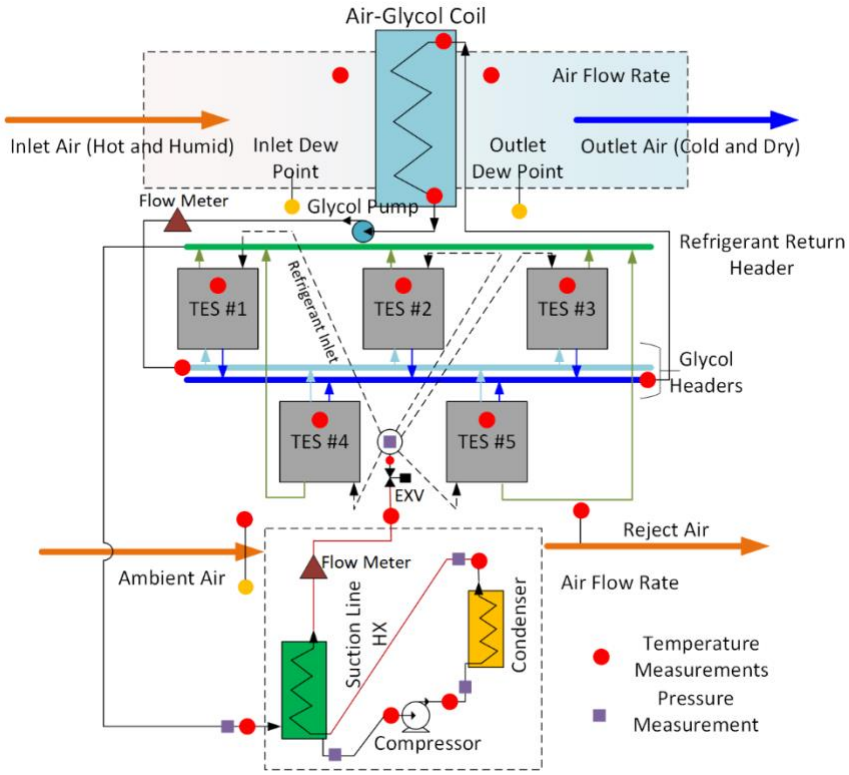

Figure 5: Schematic of the prototype 5RT system in the lab with instrumentation

This report is available at no cost from the National Renewable Energy Laboratory (NREL) at www.nrel.gov/publications.

We measured temperature and the volumetric flow rate of the glycol-water mixture in the discharge circuit. Heat transfer rate on the discharge side is calculated using:

$$\dot{Q}_{discharge} = \dot{m}_{glycol-water} Cp_{glycol-water} (|T_{in} - T_{out}|)$$

We also instrumented the thermal energy storage modules with 31 embedded thermocouples to estimate the state of charge of the system. We installed 24 surface-mounted thermocouples on tubes supplying fluids to the modules which helped quantify circuit-to-circuit fluid distribution issues.

Due to the large thermal inertia of thermal energy storage, a custom control algorithm was designed to operate the electronic expansion valve on the refrigerant circuit (Figure 6). The algorithm uses a combination of a feedforward controller based on a predictive model of the flow through the valve and a feedback controller as a corrector to achieve the setpoint of refrigerant superheat at the inlet of the compressor.

The performance of the system was characterized by charge/discharge experiments to quantify the amount of energy stored and the characteristics of the process. Steady-state heat transfer experiments helped in understating the thermal resistances present within the modules and their relative magnitude. Representative results from these experiments are discussed in the following sections of this document.

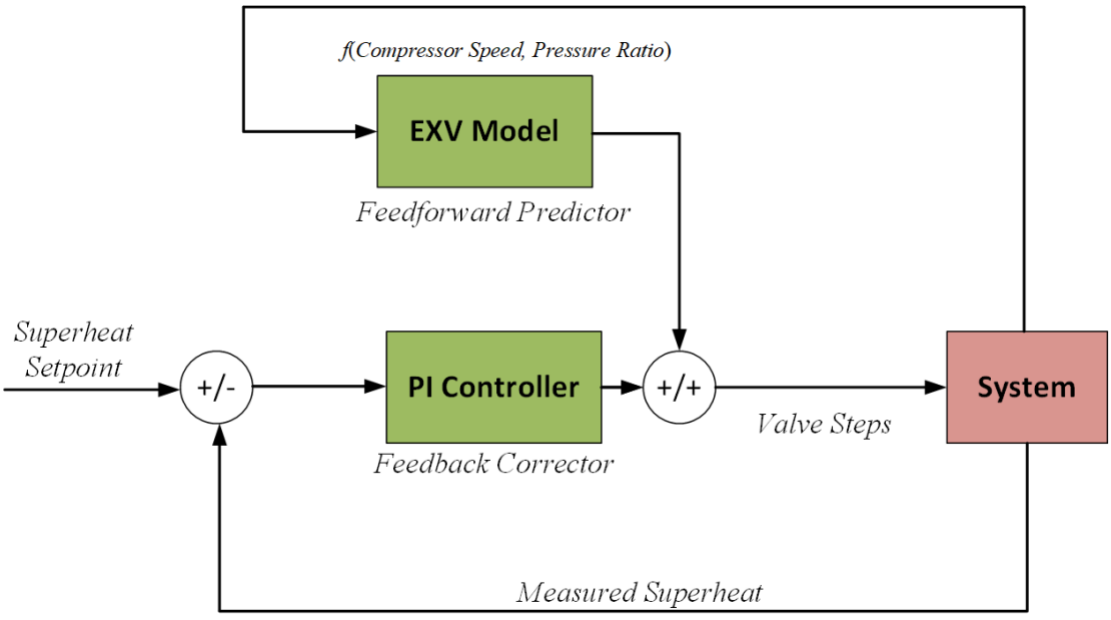

Figure 6: Control algorithm for the electronic expansion valve

This report is available at no cost from the National Renewable Energy Laboratory (NREL) at www.nrel.gov/publications.

During charging, the refrigerant circuit was operated to provide cold refrigerant to store energy in the thermal energy storage modules. The system was charged at a constant refrigerant temperature of -2°C, and condenser air temperature of 35°C and ~4500 CFM. As the system SOC increased during charging, the refrigerant temperature and consequently pressure would continuously decrease. To prevent reaching the low-pressure limit on the compressor and potentially reaching the freeze point of the water-glycol mixture in the discharge loop, the charging system was operated to maintain a constant refrigerant temperature (pressure) at the inlet of the compressor. The results from one of these experiments are shown below. Figure 7 shows the heat transfer rate, the total energy stored, and the COP of the system as a function of time. During charging the heat transfer rate decreased (remaining nearly constant at 2RT for the bulk of the phase-change process) as the driving temperature difference in the system decreased. The total energy stored was 6.6 RT-hr. In this process, the system COP remained at ~2.75. The COP of the system during charging is defined as:

$$COP_{charging} = \frac{\dot{Q}_{ref,TES}}{\dot{W}_{elec,condenser,fan} + \dot{W}_{elec,compressor}}$$

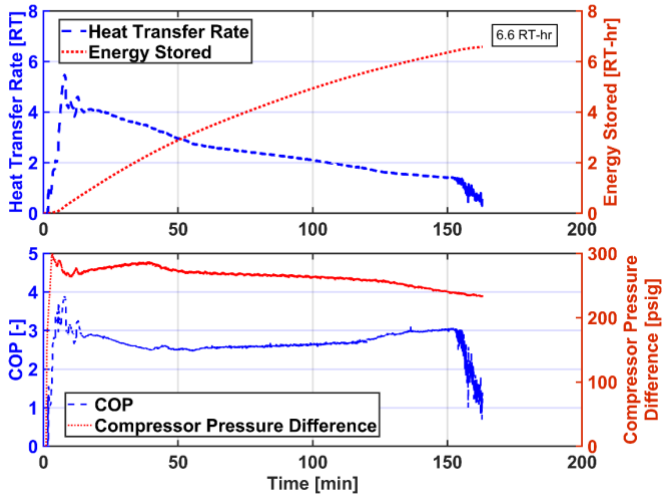

Figure 7: Heat transfer rates and energy stored in the TES heat exchanger with a saturation temperature of -6 °C.

Figure 8 shows the performance of the system as a function of the SOC. During the initial phase of charging (starting at ~15 °C isothermal conditions in the thermal energy storage modules or a SOC of 0%), the compressor operated at the maximum allowable speed of 5000 RPM) before it was modulated to maintain the refrigerant temperature. As the system SOC increased, the temperature difference between the refrigerant and the moving phase-front of the PCM decreases, leading to a decrease in the heat transfer rate. The compressor speed drops in response to this to maintain a constant refrigerant temperature. The system was charged to 100% SOC when the majority (>80%) of the embedded thermocouples inside the modules recorded a temperature below -2°C.

This report is available at no cost from the National Renewable Energy Laboratory (NREL) at www.nrel.gov/publications.

The system COP is the ratio of heat transferred into the thermal energy storage modules and the electrical input to the system (compressor and condenser fan power). The system COP during charging was ~2.75 primarily due to the low refrigerant temperature. In other experiments, the COP of the system was observed to increase at higher refrigerant temperatures, as expected. As per the original concept, the evaporator temperature was anticipated to be only 2-5°C lower than the transition temperature at the measured heat transfer rates. But due to high contact resistance, the refrigerant temperature had to be lowered to achieve the target heat transfer rate which led to lower efficiency of the refrigeration system.

After charging, the system was allowed to equilibrate overnight and discharged the next day. This allowed for isothermal initial conditions. The system was discharged at AHRI standard conditions with the inlet air set at 26.7°C dry bulb temperature, 15.8°C dew point temperature, and 2000 CFM flow rate. As the system SOC decreased during discharging, the glycol supply temperature and the air outlet temperature from the modules increased as shown in Figure 9. As the supplied air temperature increases, the performance of the system was analyzed by setting a cutoff temperature of the glycol-water mixture supplied by the modules. This also allows comparing different discharging experiments.

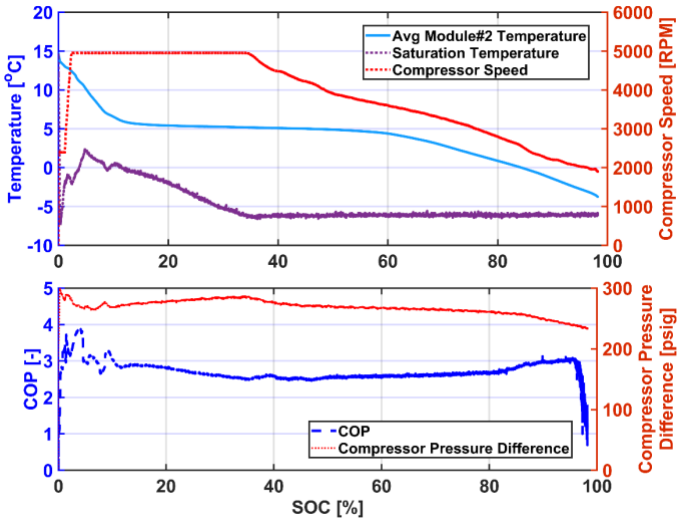

Figure 8: System performance as a function of SOC during charging at -6°C

This report is available at no cost from the National Renewable Energy Laboratory (NREL) at www.nrel.gov/publications.

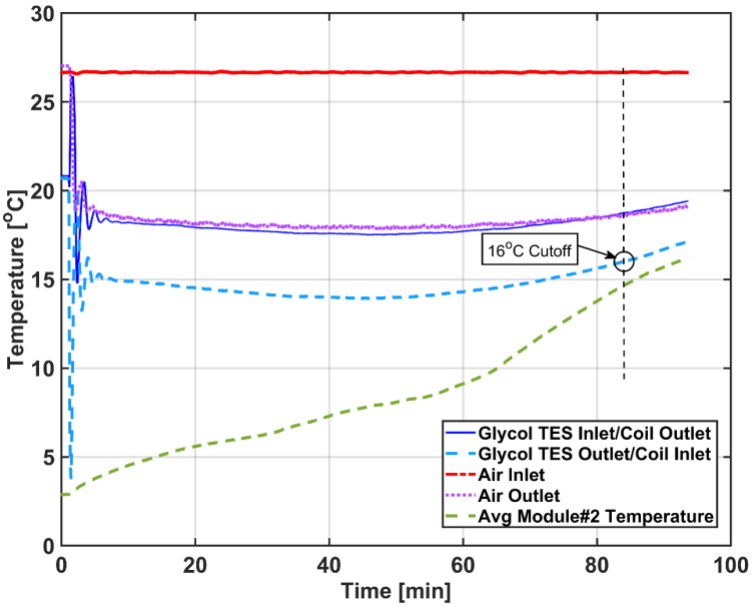

Figure 9: Air, glycol, and module temperatures during discharge at AHRI standard conditions

Figure 10 shows the heat transfer and energy discharged from the system. During the majority of the discharging, the system delivered a cooling capacity of 3.5 RT and 4.51 RT-hr of total discharged energy until reaching the cutoff glycol temperature. The system COP during discharging is calculated as the ratio of heat transferred to the glycol stream and the electrical input to the system (glycol pump and fan power). The system COP was about 15. During discharging no latent cooling (moisture removal) was observed in the air stream. This is due to the relatively high inlet glycol temperature entering the cooling coil. This high temperature was a result of higher than anticipated thermal resistance between the glycol circuit and the thermal energy storage material. As shown in Figure 9 and Figure 11, the temperature of the glycol stream supplied by the modules remained close to 14°C which was unable to condense any moisture from the airstream. With improved thermal contact between the fluid tubes and the thermal energy storage, better heat transfer rates and energy utilization can be achieved from the system.

This report is available at no cost from the National Renewable Energy Laboratory (NREL) at www.nrel.gov/publications.

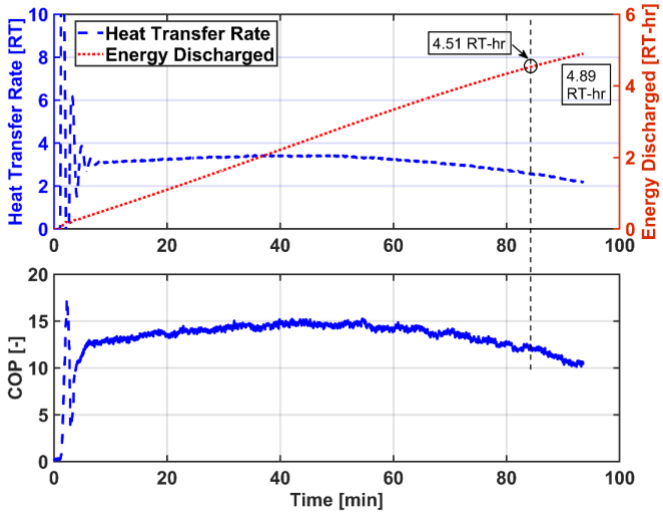

Figure 10: Heat transfer and energy storage performance of the system during discharge at AHRI standard conditions

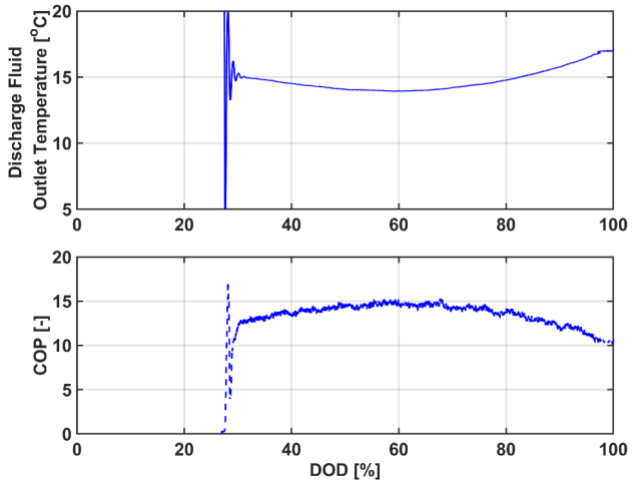

Figure 11: Glycol outlet temperature and COP as a function of the depth of discharge (DOD) at AHRI standard conditions

This report is available at no cost from the National Renewable Energy Laboratory (NREL) at www.nrel.gov/publications.

Task 3: Gen-2 design

Task Summary: *Based on results from Task 2 experimental results, NREL will update the models for the PCM thermal storage module and HVAC system. The updated model, along with lessons learned from the first prototype build and characterization, will be used to update the new PCC design.*

In addition to the serpentine design, we also investigated the use of aluminum microchannels for the charge and discharge fluids. Multi-port extruded (MPE) aluminum channels are commonly used in air conditioning systems to reduce air-side pressure drop and increase heat transfer coefficients. The channels have flat top and bottom surfaces that contain many microchannel passages to improve the structural stability of the pressurized tube and increase heat transfer rates. An example of a multi-port microchannel tube is shown in Figure 12. Replacing the round tubes in the serpentine design with MPE channels could have many advantages for the TES module because they will create a flat contact surface between the channels and the composite PCM (potentially reducing contact resistance) and allow for the refrigerant and glycol channels to be in direct contact.

Figure 12: A flat microchannel extruded tube (source: Tai Xing Group)

The proposed microchannel design consists of refrigerant and glycol-water MPEs that are stacked directly on top of each other. The two fluid are routed through the heat exchanger in a single counterflow pass. The total length and width of the MPEs are equal to the length and width of the module, which was set to match the dimensions of the round-tube design (18 inches long and 20.5 inches wide). Each channel pair is sandwiched between two 35-mm thick composite PCM slabs where heat is stored or extracted. The total storage capacity can be scaled by adding glycol-refrigerant tube pairs and the surrounding COMOPSITE PCM, where fluid from the chiller and load is equally distributed to the channels with manifolds. The number of channels in the system were chosen to match the storage capacity of the serpentine design (21.5 kWh or 6.11 ton-h), resulting in about 54 composite PCM slabs.

A 2-D transient numerical model was developed to characterize a single unit cell consisting of two fluid channels and two PCM slabs. The model discretizes the system into smaller sub-volumes to track the local temperature and enthalpy changes throughout the discharge process. The model has four types of sub-volumes, or nodes, as shown in Figure 13. The phase change material is discretized in both the x- and y-directions into 400 nodes. The refrigerant, glycol-water, and aluminum walls are discretized into 20 nodes in the x-direction (fluid flow direction). The hot and cold channel aluminum walls are assumed to be isothermal within a node, which

This report is available at no cost from the National Renewable Energy Laboratory (NREL) at www.nrel.gov/publications.

allows heat to spread throughout the finned structure. The conduction heat transfer rates between PCM nodes is calculated with a discretized version of Fourier's law, accounting for directional differences in the thermal conductivity of the composite PCM. Heat transfer rates between different types of nodes are calculated by considering all relevant resistances, including fluid convection, contact, and conduction resistances. The enthalpy or temperature changes with time are calculated using an energy balance, shown in the equations in Figure 13. All nodes have a thermal storage term except for the refrigerant nodes, which can change temperature effectively instantaneously with changes in pressure. The enthalpy and temperature of each node is calculated with numerical integration using the explicit Euler approach.

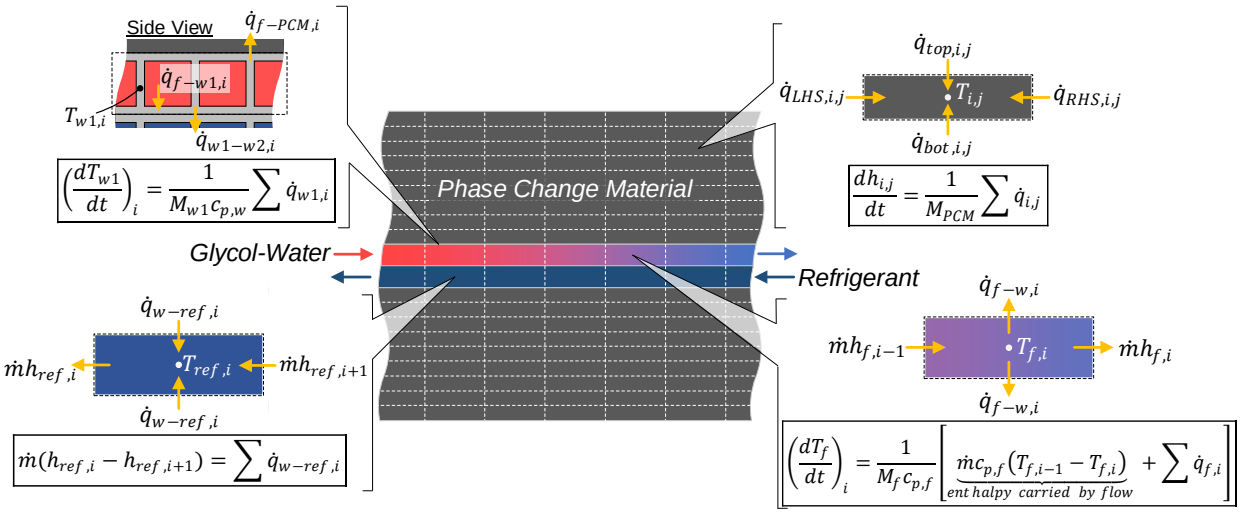

Figure 13: A schematic representation of the different types of nodes in the microchannel heat exchanger model. The dashed boxes indicate the boundaries of the nodes and all yellow arrows show energy flows in and out of the control volumes. The equations show the energy balance for each type of node.

To simplify the calculations, the model assumes:

- The thermal resistance in the aluminum walls is negligible and the wall temperature is constant in each node.
- The thermal contact resistance between the composite PCM and the tube wall is 6×10-4 K m-2 W-1, which is 3x lower than the serpentine design.
- The contact resistance between the hot and cold channel walls is 6×10-5 K m-2 W-1
- The multi-port extruded tubes have 150 ports each, resulting in channel hydraulic diameters of 2.6 mm (this tube geometry has not been optimized).
- The refrigerant heat transfer coefficient in each node is equal to the average heat transfer coefficient over the entire quality range calculated using the Shah (1982) correlation.
- The heat transfer coefficient in the glycol-water channels is calculated based on the fluid properties in each node using appropriate correlations for developing and fully developed laminar, turbulent, and transitional flow.

This report is available at no cost from the National Renewable Energy Laboratory (NREL) at www.nrel.gov/publications.

The glycol-water heat transfer rate was held constant by maintaining a constant temperature difference between the inlet and outlet. During discharge, the inlet glycol temperature increases to compensate for the higher internal PCM resistances. The saturation pressure of the refrigerant stream was set so that the fluid exits at a quality of 1. The required saturation pressure was calculated through iteration at each timestep. The control procedures for the two fluid streams are identical to the round-tube analysis.

Microchannel TES results and discussion

The microchannel design offers several advantages over the original round-tube design, including a lower fluid inventory, a larger internal tube surface area (2.9x higher), and lower resistances between the fluid streams (channels are in direct contact) and between the channel walls and composite PCM (3x reduction in the contact resistance). However, the surface area between the channel walls and composite PCM is lower in the microchannel design (6.45 m^2 vs 8.26 m^2) because only half of the flat channel is in contact with the storage medium. The reduced surface area is partially mitigated by the ability for heat to spread through the finned microchannel structures.

The performance of the microchannel heat exchanger design was quantified for 36 different hybrid charge/discharge rates. An example case is described below, with a charge rate from the refrigerant of about 11.8 kW (3.4 tons) and a discharge rate from the glycol of about 3.5 kW (1.0 ton). The SOC throughout the charging process is similar for the two designs, as shown in Figure 14. This is expected because the capacity and net heat transfer rate from the composite PCM are nearly identical in the two components. The only differences arise in the amount of thermal storage outside of the composite PCM. The serpentine round-tube design has a larger fluid inventory that requires more thermal energy to heat it up. The larger amount of thermal storage in the fluid results in slightly longer charging times.

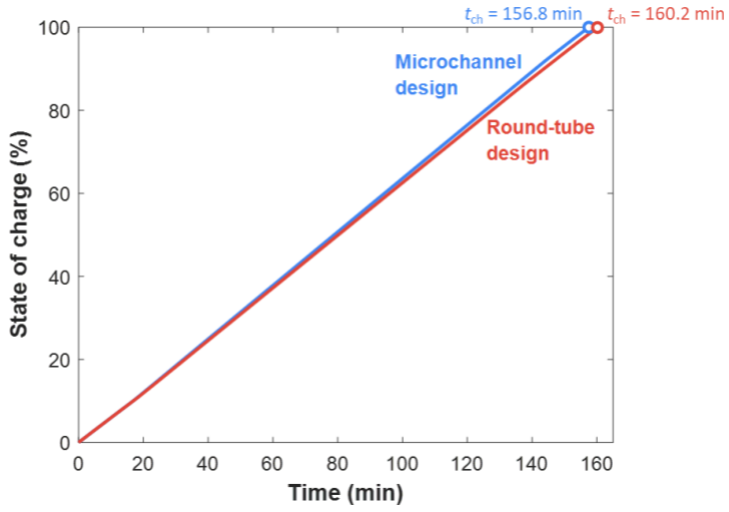

Figure 14: The progression of the PCM state of charge with time when the system is charging at a net rate of 8.3 kW (2.4 tons).

This report is available at no cost from the National Renewable Energy Laboratory (NREL) at www.nrel.gov/publications.

Although the SOC is similar between the two designs, the change in the PCM state is accomplished at different fluid temperatures. The glycol outlet and refrigerant temperatures during the charging process are shown in Figure 15. The lower resistances in the microchannel design result in lower refrigerant temperatures and higher glycol outlet temperatures. The improved performance has system-level benefits because the compressor operates more efficiently. The system results are discussed more in Section 7.

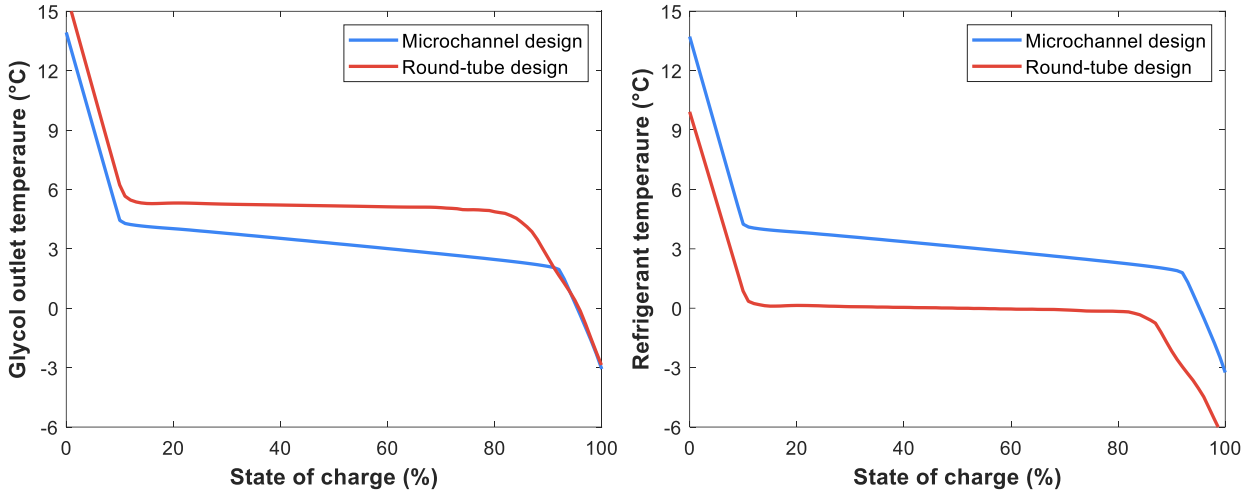

Figure 15: The (left) glycol outlet temperatures and (right) refrigerant saturation temperatures of the two proposed designs during the charging process when the net charge rate is 8.3 kW (2.4 tons).

Task 4: Gen-2 prototype characterization and integration experiments

Task Summary: *Under this task, NET Energy and its OEM partners will fabricate prototypes of the PCM thermal storage modules and incorporate them into the existing HVAC system and deliver them to NREL. NREL will characterize the performance of these prototypes in its laboratory, share these results with NET Energy, and use the results to validate or update their numerical models.*

The model described in Task 3 was validated with a stacked microchannel TES heat exchanger coupled to two glycol streams. The microchannel heat exchangers carry hot and cold propylene glycol - water through the component (Figure 16). Each array contains 9 tubes containing 135 individual microchannel ports with hydraulic diameters of 1.3 mm. The flow is split evenly into the microchannel ports by a common manifold. Thermal paste was added between the two arrays to reduce the contact resistance. Rectangular slabs (41.9 cm × 25.9 cm × 3.6 cm) of a graphite/tetradecane PCC are placed above and below the microchannel arrays. We found that tetradecane leaked out of the graphite material when cycled, so each slab was encapsulated in a heat-sealed Mylar bag. The bag increases the surface resistance but avoids the loss of capacity over time.

This report is available at no cost from the National Renewable Energy Laboratory (NREL) at www.nrel.gov/publications.

Figure 16: The microchannel heat exchanger used in the model validation experiments. Each microchannel array is attached to a common manifold that distributes the refrigerant to the microchannel ports. The microchannel tubes are bent at a 45-degree angle at both ends to allow room for the manifolds. The PCC slabs are placed above and below these microchannel arrays to provide thermal storage.

The TES heat exchanger ("test section") was placed in the facility shown in Figure 17. The inlet temperature and flow rate of the glycol mixture is controlled using constant temperature circulating baths (Fisher Scientific 6200 R35), a 1-kW external heater (Watlow FLUENT) and a DC variable speed diaphragm pump. The hot fluid loop (or discharge loop) can add heat to the cold loop and/or the PCC by supplying fluid at a constant inlet temperature (controlled with the temperature bath) or a constant power. For all constant power tests, the fluid temperature difference was set at 4.5°C and the flow rate was varied to achieve the desired heat transfer rate. The cold loop (or charge loop) can remove heat from the discharge loop and/or the PCC by supplying a constant temperature fluid to the test section inlet (controlled with the temperature bath). Pressure was applied to the top of the test section with a screw clamp to improve the thermal contact between the channel walls and the PCC. The tests were run with 4 psi of applied pressure, which was measured with a load cell (Omega LC304-5K).

We evaluated the performance of the test section at a variety of charge and discharge rates. The operating conditions for each run are shown in Table 1. The discharge loop was run at a constant power for all cases. Although the heat transfer rate from the charge loop could not be controlled at a constant power, the inlet conditions were set so that the average charge rates were near the target. Cases 1-5 started from the fully charged state and cases 6-10 started at the fully discharged state. The model described above was modified to include two glycol streams and to account for gaps between parallel MPE tubes. The experimentally measured inlet temperatures and flow rates were fed into the model and the measured fluid outlet and PCC temperatures were compared to the model to validate the results.

This report is available at no cost from the National Renewable Energy Laboratory (NREL) at www.nrel.gov/publications.

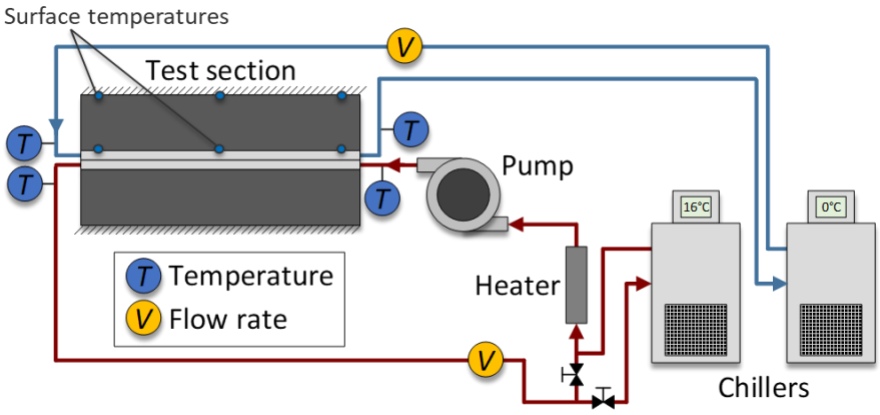

Figure 17: A schematic of the experimental facility where the instruments marked with T and V are thermocouples and a volumetric flow meter, respectively.

Table 1: The target operating conditions for the validation experiments

	Target conditions			Discharge circuit		Charge circuit	
	Discharge	Average Charge	Run time	Flow Rate	Temperature Difference	Flow Rate	Inlet Temperature
Case 1	325 W	0 W	1 hr	1.09 L/min	4.5°C	-	-
Case 2	325 W	160 W	2 hr	1.09 L/min	4.5°C	1 L/min	6.0°C
Case 3	325 W	217 W	3 hr	1.09 L/min	4.5°C	1 L/min	4.0°C
Case 4	325 W	325 W	-	1.09 L/min	4.5°C	1 L/min	0.0°C
Case 5	485 W	320 W	2 hr	1.46 L/min	5.0°C	0.8 L/min	3.8°C
Case 6	0 W	325 W	1 hr	-	-	1 L/min	-5.2°C
Case 7	160 W	325 W	2 hr	0.54 L/min	4.5°C	1 L/min	-4.0°C
Case 8	217 W	325 W	3 hr	0.73 L/min	4.5°C	1 L/min	-2.4°C
Case 9	325 W	433 W	3 hr	1.09 L/min	4.5°C	1 L/min	-4.5°C
Case 10	325 W	325 W	-	1.09 L/min	4.5°C	1 L/min	8.0°C

Experimental/Model Comparison

The microchannel heat exchanger was first evaluated under steady state conditions to determine the contact resistance between the hot and cold fluid channels. We calculated a contact resistance of approximately 3×10^{-4} K m^2 W^{-1}, which was used to update the glycol-glycol finite difference model. The channel-channel contact resistance was not changed in the refrigerant-glycol model because we should be able to reduce this resistance in the final design by brazing the arrays together or extruding both tubes as one part.

Before we compared the model to the experimental results, we examined the PCC properties, which have a large impact on the device performance. First, we changed the density from 836 to 872 kg m^{-3} to match the volume and mass of the uncycled slab. We then looked at the surface temperature probes and compared the measurements to our expectations. Initially we assumed that the graphite/tetradecane had a transition temperature of 4.6°C and a temperature glide of 0.5°C based on earlier DSC measurements. The phase change temperatures can be identified by examining the surface thermocouple measurements between the PCC and insulation (Figure 18a) since the heat flows through the top surface are minimal. Here the phase change endset temperature is closer to 6°C than the originally assumed 4.85°C. We investigated these values further with temperature-history experiments with tetradecane. These experiments found that the transition temperature and temperature glide were closer to 5.4°C and 1°C, respectively. We changed the h-

This report is available at no cost from the National Renewable Energy Laboratory (NREL) at www.nrel.gov/publications.

T curve to account for these differences. The comparison between the modeled and measured PCC surface temperatures are shown in Figure 18. We adjusted the model values to account for the fact that the sensors we placed on the outside of the Mylar encapsulation. The trends are similar between the model and the experiment, although the PCC temperature drops more quickly near the insulation surface. This may be due to differences in the PCC properties (not as sharp of a transition at the onset point).

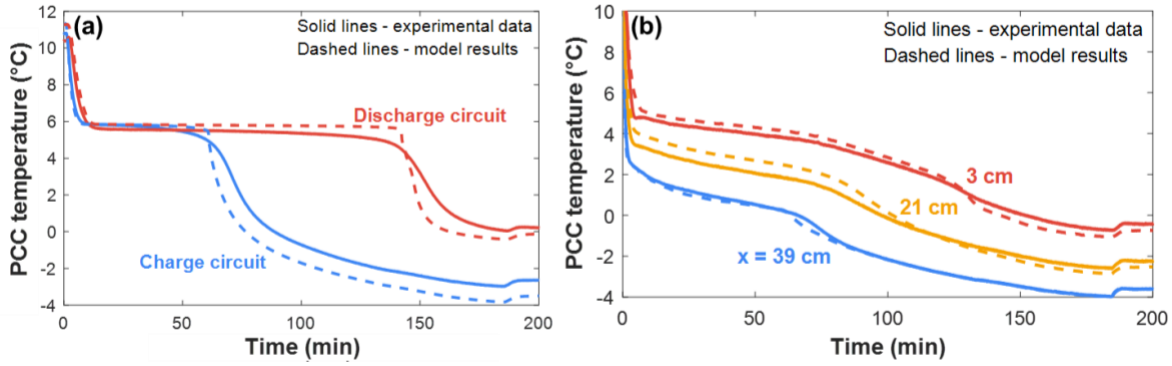

Figure 18: The measured PCC temperatures at the surface (a) between the PCC and the insulation and (b) between the PCC and the microchannel wall when the average charge rate is 325 W and the discharge rate is 160 W.

The model was then compared to the experimental data for a range of discharge rates. The results are shown in Figure 19. The model results align well with the experimental data, showing both the correct trends and temperature values. The absolute average deviation for the discharge and charge circuit outlet temperatures were 0.27 and 0.29°C, respectively. This shows that the model can accurately predict the outlet states of the fluid.

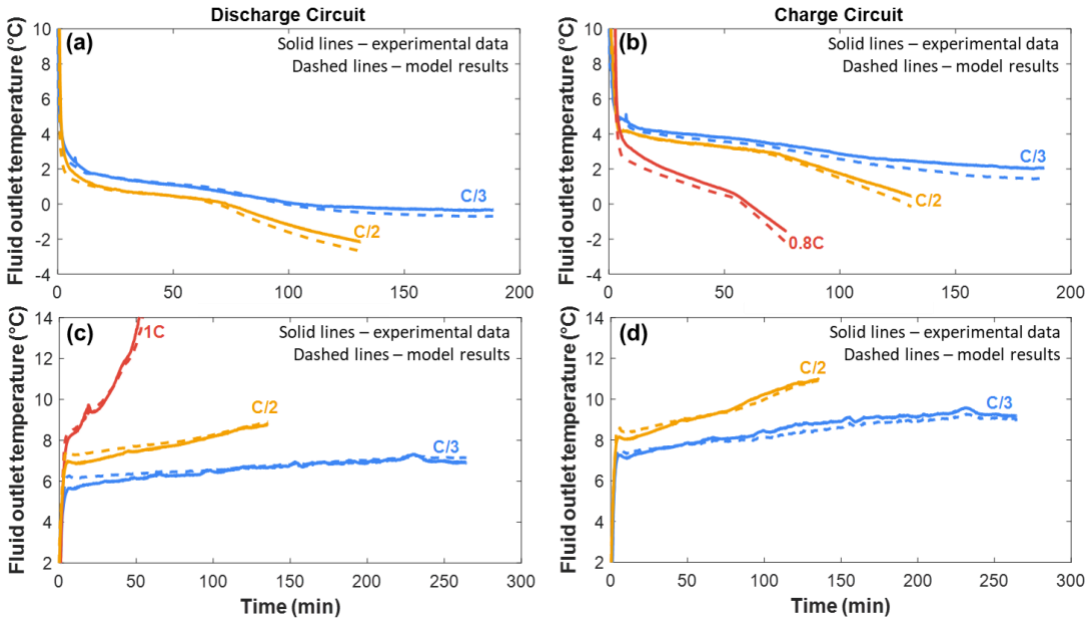

Figure 19: The fluid outlet temperatures from the (a) discharge circuit and (b) charge circuit while charging the device at different rates (cases 1-3) and the fluid outlet temperatures from the (c) discharge circuit and (d) charge circuit while discharging the device at different rates (cases 6-9).

This report is available at no cost from the National Renewable Energy Laboratory (NREL) at www.nrel.gov/publications.

Comparison to Previous Design

With the validated model, we were able to compare the microchannel design to the experimental data collected with the glycol-coupled serpentine component (Goyal *et al.*, 2021). The capacity in the model was set to match the serpentine component, and the flow rates and temperature differences across each fluid stream were set to match the experimental targets. The experimental serpentine results are compared to the microchannel model results in Figure 20 while only discharging the device (charge circuit was turned off). The results are similar, with the microchannel device performing slightly better, particularly at high power rates. For example, at 1.51 C (5.3 kW) the microchannel component can extract nearly 3 kWh of capacity from the component, whereas the serpentine device can only use about 2 kWh before it reaches the cutoff.

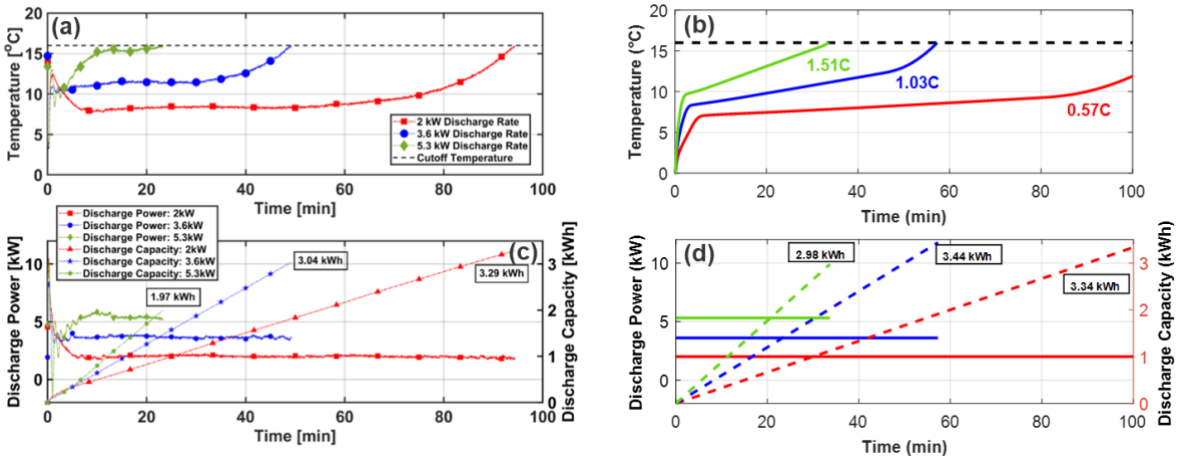

Figure 20: Discharge experiments: Comparison between the discharge circuit fluid outlet temperatures (a) experimentally measured in the serpentine design and (b) modeled with the validated microchannel finite difference simulation. The discharge power and capacity before the outlet temperature reaches the cutoff (16°C) in the (c) serpentine experiments and from the (d) microchannel model are also shown.

The microchannel design has a larger impact when the device is discharged in hybrid mode, as shown in Figure 21. Again, the capacity, flow rates and temperature differences from the serpentine experiments were used in the microchannel model to compare their performance. In this case, the microchannel design performs sustainably better because of the good thermal contact between fluid channels. The charge fluid inlet temperature (blue line in Figure 21 a and b) is much higher than the serpentine design, meaning that the efficiency of the charging system will improve with the new component. Additionally, the discharge circuit outlet temperature remains below the cutoff temperature for longer, which will result in a high useable system capacity.

This report is available at no cost from the National Renewable Energy Laboratory (NREL) at www.nrel.gov/publications.

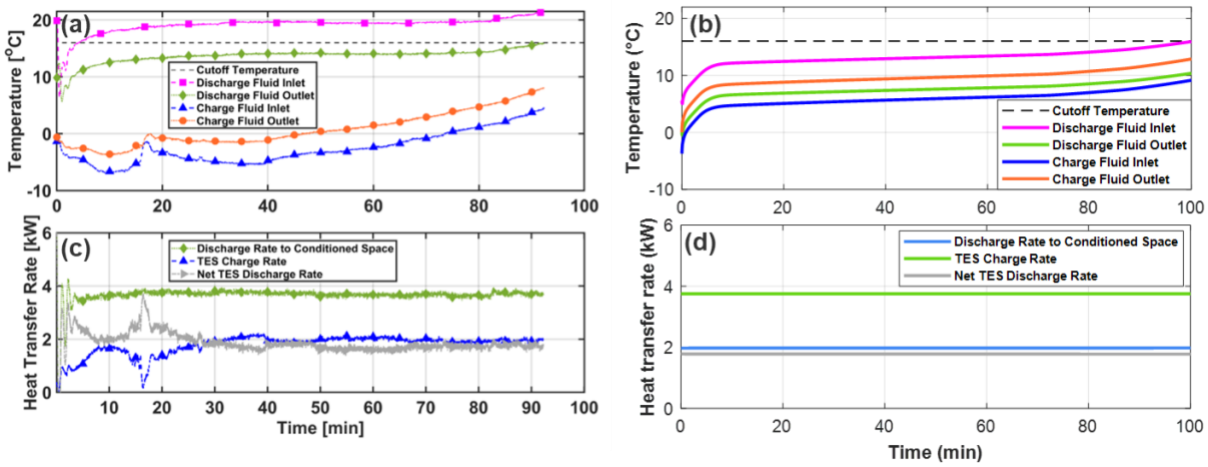

Figure 21: Hybrid discharge experiment: Comparison between the discharge and charge circuit fluid outlet temperatures (a) experimentally measured in the serpentine design and (b) modeled with the validated microchannel finite difference simulation. The discharge, charge, and net heat transfer rates for the (c) serpentine experiments and (d) microchannel model are also shown.

Task 5: Building modeling and scenario simulations

Task Summary: *With updated thermal storage module and HVAC system models, NREL will run building simulations for different scenarios. These modeling results will be used to update target market locations and economic estimates.*

We investigated the performance of the hybrid TES RTU for a retail strip mall building. This included two climates: Los Angeles, CA (climate zone 3B), a hot climate with relatively large diurnal temperature swings, and Baltimore, MD (climate zone 4A), a warm/humid climate with smaller diurnal temperature swings. The specific scenarios are shown in Table 2 below, which include one serpentine design case for each climate, and four microchannel cases with different capacities and PCM transition temperatures.

This report is available at no cost from the National Renewable Energy Laboratory (NREL) at www.nrel.gov/publications.

Table 2: Scenarios investigated for comparing the hybrid TES system to the baseline variable-speed RTU

Scenario	Climate	TES design	PCM transition temperature, Tt	TES capacity
			°C	tonh
1	Los Angeles, CA	Serpentine	4.5	6.9
2		Microchannel	4.5	6.9
3		Microchannel	4.5	4.0
4		Microchannel	10.0	6.9
5		Microchannel	10.0	4.0
6	Baltimore, MD	Serpentine	4.5	6.9
7		Microchannel	4.5	6.9
8		Microchannel	4.5	4.0
9		Microchannel	10.0	6.9
10		Microchannel	10.0	4.0

The building model is based on the DOE Reference Building for a retail strip mall, which matches building practices from roughly 2010-2015. The load profile was scaled to a single 5-ton RTU, assuming the system is ~20% oversized. The load profiles for Los Angeles and Baltimore are shown in Figure 22. Note that the thermostat setpoint in the building model is increased at night, which means there is no building load from 9pm-6am.

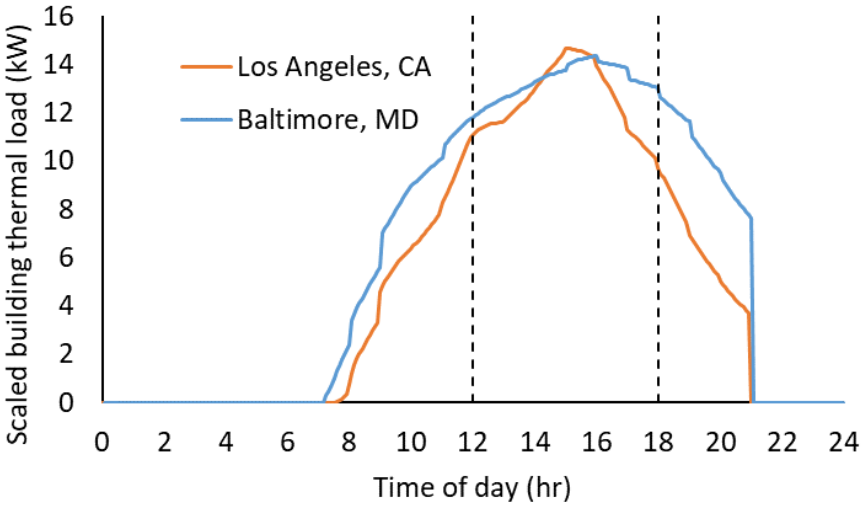

Figure 22: Building load profiles, scaled to align with a 5-ton RTU load.

This report is available at no cost from the National Renewable Energy Laboratory (NREL) at www.nrel.gov/publications.

Hybrid TES RTU system - results and discussion

The 24-hour simulation results are shown in Figures 23 and 24 for Los Angeles and Baltimore, respectively. There are six sets of graphs in each figure, including (a) one for the baseline RTU, and (b) five for the hybrid TES RTU. The black dashed lines show the assumed 6 h peak-demand period between noon and 6pm.

The graph for the baseline RTU shows the total HVAC load and the heat absorbed by the evaporator, which meets the HVAC load, including cycling to meet the load during low-load periods. The blue line shows the total RTU power, which reaches its peak during the peak-demand period.

The five graphs for the hybrid TES RTU show the same HVAC load as the baseline, the heat absorbed by the cooling coil, which meets this HVAC load, and the RTU energy use (blue line). These five plots also show the heat transfer into the boiling refrigerant (light blue line), and the heat being storage in the TES (dashed grey line). Each timestep, these energy flows balance:

$$Q_{TES,net} = Q_{evaporator} - Q_{CoolingCoil}$$

An inset graph in the top left shows the TES SOC over the 24 h period. The control strategy charges the TES from the initial 25% to ~85%, and then maintains that SOC until just before the peak period. This keeps the evaporator temperature lower, and improves heat-pump efficiency during the morning hours where cooling is needed, but the battery is not being charged or discharged. The TES is then charged to >95% just before noon.

During the peak period, the compressor speed changes to maintain a constant power for the entire RTU (compressor + fans + pump). For a fixed compressor power, the cooling provided by the refrigerant ($Q_{evaporator}$) decreases as the ambient temperature increases. This causes the dip in $Q_{evaporator}$ near 3pm. This drop is more pronounced in Los Angeles because the ambient temperature is higher than in Baltimore. The TES makes up the difference ($Q_{TES,net}$) between the cooling provided by the refrigerant and that being delivered to the cooling coil.

The peak power from noon-6pm and the electric energy use over the 24 h period are summarized in Table 4. Compared to the serpentine design, using microchannels reduces the peak power by a further 17% in Los Angeles and 19% in Baltimore. It also reduces total energy use over the day. Alternatively, the peak-power reduction can be kept the same as the serpentine design using microchannels, but with a much smaller battery: ~4 tonh, and also with a smaller energy penalty.

Changing the transition temperature of the PCM to 10 °C can still provide the same peak-load reduction as the 4.5 C, but with lower 24 h energy use. In fact, the energy use for the baseline variable-speed RTU and the hybrid TES are nearly the same when using a PCM with a transition temperature near 10 °C.

This report is available at no cost from the National Renewable Energy Laboratory (NREL) at www.nrel.gov/publications.

The differences in energy use are driven by the evaporator and condenser temperatures, and the evaporator temperature is the primary difference between the three TES heat exchanger designs. Table 5 shows these evaporator temperatures for the cases in Los Angeles. There are three key points to take away from this table. First, the evaporator temperature depends on the TES SOC of, with high SOC (>90% just before noon) requiring the lowest evaporator temperature, and low SOC (~10%) allowing for much higher evaporator temperatures. This is also shown in Figure 15, which shows the evaporator and glycol temperatures from 0% to 100% state of charge. Second, the evaporator temperature increases when using the microchannel design because it brings the glycol and refrigerant next to each other, rather than being separated by the composite PCM. Finally, increasing the PCM transition temperature (10 °C from 4.5 °C) increases the evaporator temperature up by a similar amount (~5.5 °C) when the SOC is in the middle range (PCM is changing phase), but has a smaller impact at the ends (<10% and >90% SOC).

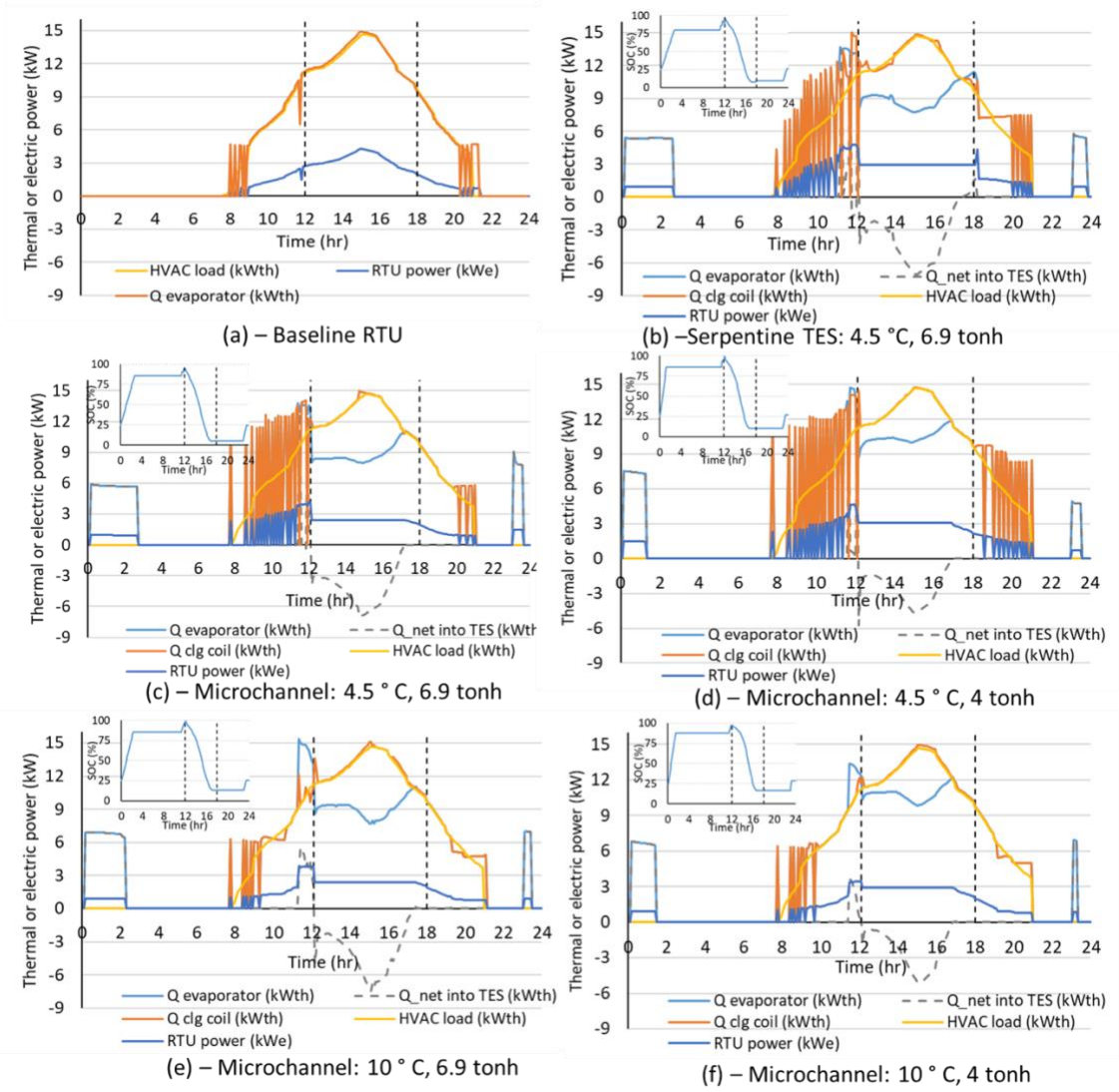

Figure 23: RTU energy use for the peak day in Los Angeles, CA for (a) baseline RTU, (b) hybrid serpentine TES RTU with 6.9 tonh and Tt = 4.5 °C, hybrid microchannel TES RTU with (c) 6.9 tonh and Tt = 4.5 °C, (d) 4 tonh and Tt = 4.5 °C, (e) 6.9 tonh and Tt = 10 °C, and (f) 4 tonh and Tt = 10 °C.

This report is available at no cost from the National Renewable Energy Laboratory (NREL) at www.nrel.gov/publications.

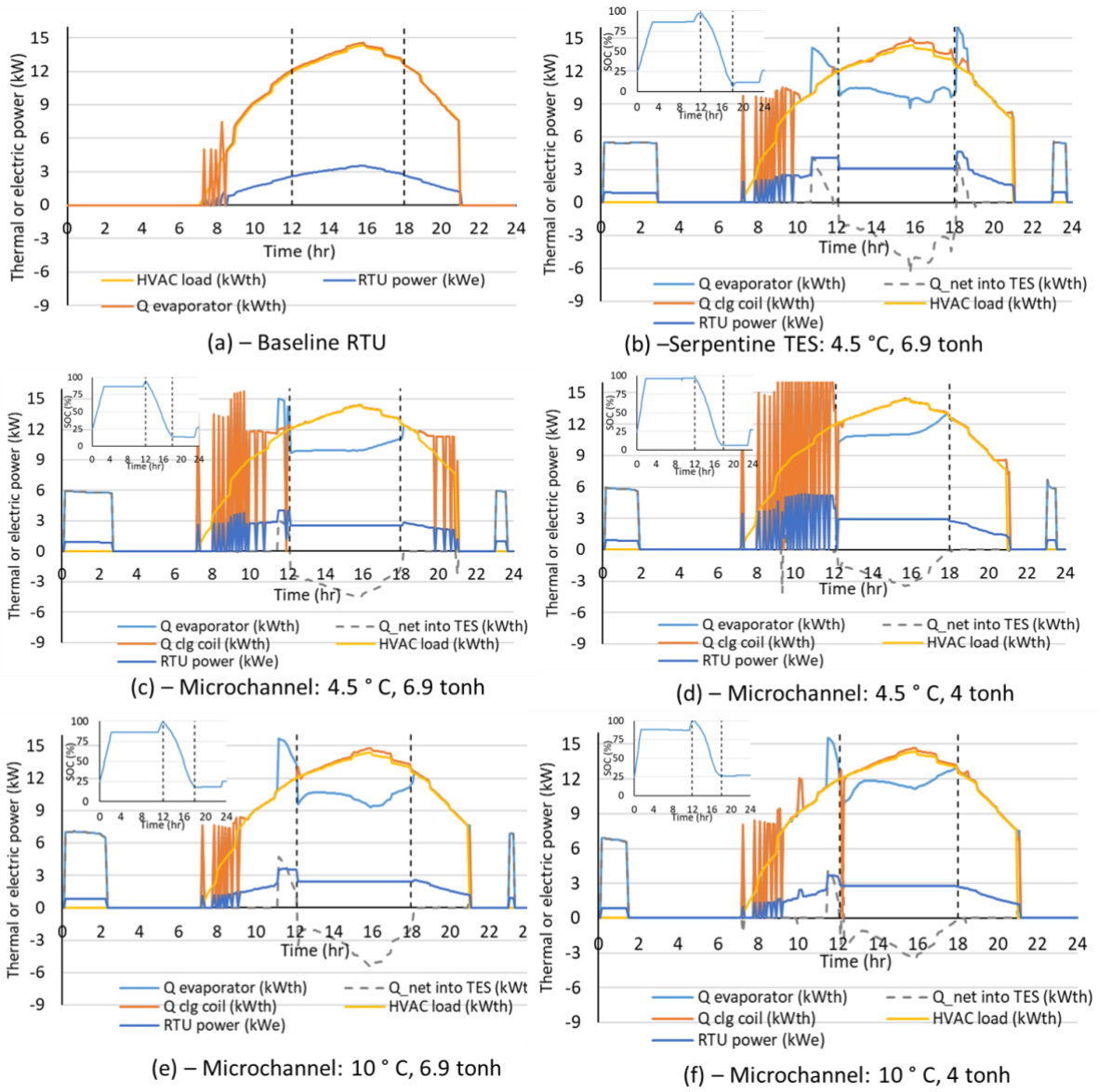

Figure 24: RTU energy use for the peak day in Baltimore, MD for (a) baseline RTU, (b) hybrid serpentine TES RTU with 6.9 tonh and Tt = 4.5 °C, hybrid microchannel TES RTU with (c) 6.9 tonh and Tt = 4.5 °C, (d) 4 tonh and Tt = 4.5 °C, (e) 6.9 tonh and Tt = 10 °C, and (f) 4 tonh and Tt = 10 °C.

This report is available at no cost from the National Renewable Energy Laboratory (NREL) at www.nrel.gov/publications.

Task 6: Path to Market

Task Summary: *This task will provide the necessary technical information that can help develop the commercialization strategy. The following attributes will be developed based on engineering modeling results and market adoption requirements.*

- *Targeted climate region / Building Profile / Grid Integration –modeling results will be leveraged to determine in which climate regions / buildings / and grids the proposed technology will have the most desirable impacts.*
- *Performance Indices - the following are example of performance metrics that can increase market adoption in targeted applications.*
    - *System efficiency*
    - *TES round trip efficiency and charging/discharging duration*
    - *Instantaneous and integrated capacities*
    - *Connectivity and demand response capabilities will be evaluated based on economic benefits offered by utilities.*
- *Information dissemination – this task will explore partnerships with utilities to initiate new assessment projects to qualify the technology for inclusion in the incentive programs. Additionally, this task will spread the awareness of the project through various venues including conferences and journal publications.*

As part of Task 6, NREL and NETenergy held meetings with various electric utilities about the benefits of the technology for managing peak load. We also presented on this technology at venues attended by several HVAC manufacturers, including the Herrick Refrigeration and Air Conditioning Conference, the ASME Summer Heat Transfer Conference, as well as the Building Technologies Office Peer Review.

Task 7: Final Evaluation

Task Summary: *Following Task 6, each party will perform its own final evaluation of the HVAC + thermal storage system and the parties will meet in good faith to discuss whether to continue working on the technology in future phases and in what capacity*

This task was originally proposed for this CRADA project, but this Gen-2 prototype was not delivered to NREL for evaluation.

Task 8 and 9: Modeling and design of high-power PCM heat exchanger, and bench-scale experimental validation

For this task, we designed two thermal storage prototypes with extremely fast discharge rates (discharge in ~5 minutes). The first prototype used glycol as the working fluid, with a target discharge power of 1 kW and a total energy of 0.1 kWh. The second used two-phase ammonia as the heat transfer fluid, with a target power of 25 kW and a total energy of 1 kWh.

This report is available at no cost from the National Renewable Energy Laboratory (NREL) at www.nrel.gov/publications.

The model used for the glycol prototype was similar to the one used for Task 3 (Figure 13), but with only one fluid channel. The prototype was characterized using the experimental setup from Task 4 (Figure 17), but again with only one channel. The experimental results are shown in **Figure *25***, showing good agreement between model and experiment and that we can achieve ~3-minute discharge and maintain temperature below 15 °C.

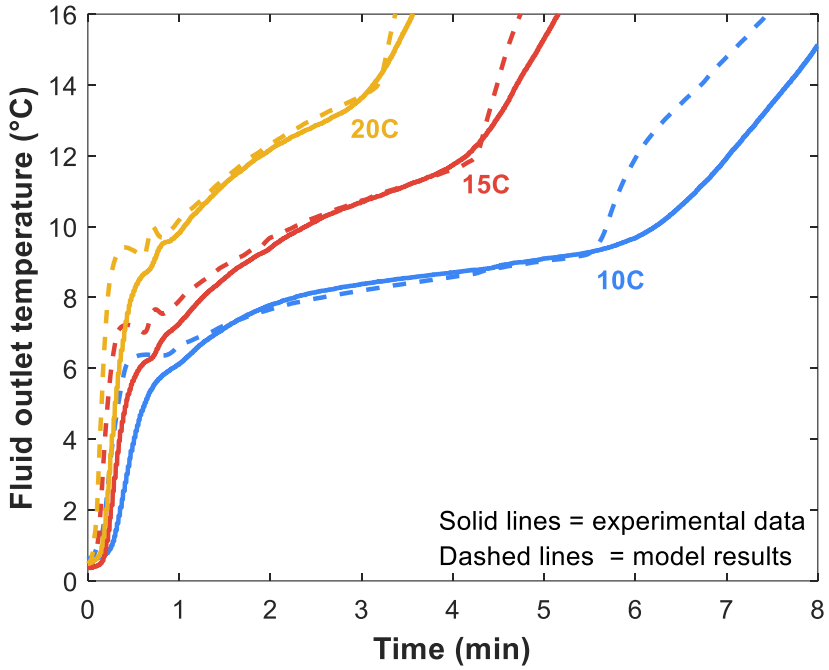

Figure 25: Discharge performance of high-power glycol prototype, with discharge periods of 1/10th hour, 1/15th hour, and 1/20th hour. Fluid outlet temperature rises to maintain constant power, and we generally see good agreement between the model and the experiment.

For the second prototype, the model from Task 3 was modified to use a single channel with two-phase ammonia as the heat transfer fluid. The modeling results show a discharge period of ~3 minutes, with the temperature maintained below 16 °C (Figure 26). However, the discharge power does drop after 2.5 minutes, as shown in Figure 27.

This report is available at no cost from the National Renewable Energy Laboratory (NREL) at www.nrel.gov/publications.

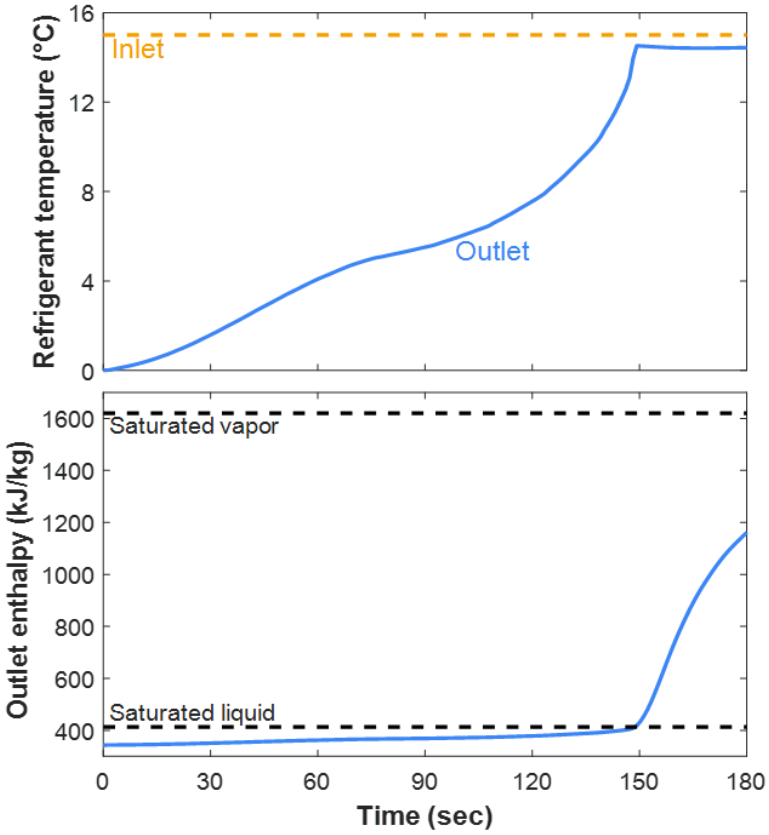

Figure 26: Modeled results for two-phase ammonia prototype design, including refrigerant temperature and pressure during discharge.

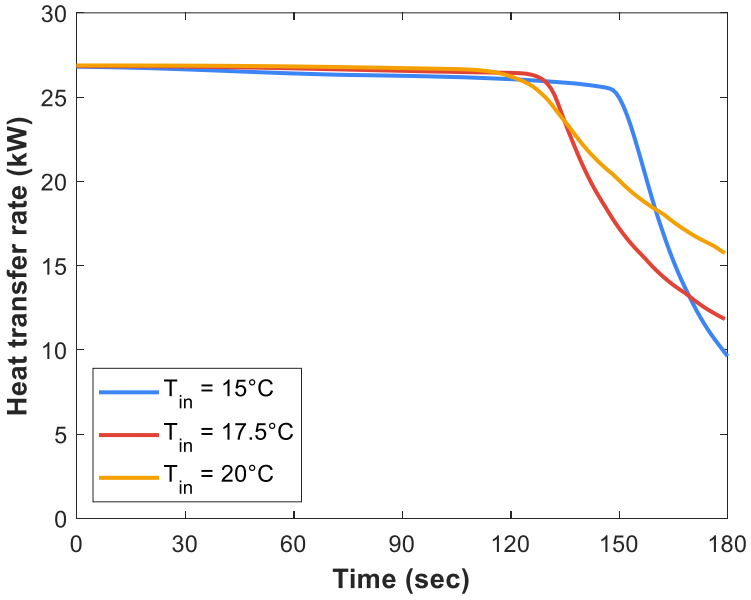

Figure 27: Modeled results for two-phase ammonia prototype design—heat transfer rate at three inlet temperatures.

This report is available at no cost from the National Renewable Energy Laboratory (NREL) at www.nrel.gov/publications.

References:

Goyal, A., E. Kozubal, J. Woods, M. Nofal, S. Al-Hallaj. “Design and performance evaluation of a dual-circuit thermal energy storage module for air conditioners”. *Applied Energy*. 292 (2021) 116843.

Goyal, A., E. Kozubal, J. Woods (2021). “Integrated thermal energy storage system for air conditioners with phase-change composites”. Presented at [International Refrigeration and Air Conditioning Conference]. West Lafayette, IN. Paper 2116.

Subject Inventions Listing:

None

ROI#:

None

This report is available at no cost from the National Renewable Energy Laboratory (NREL) at www.nrel.gov/publications.